Astronomy & Astrophysics manuscript no. Klein˙al˙23783˙arxiv
March 11, 2014

The relativistic solar particle event of 2005 January 20: prompt and delayed particle acceleration

K.-L. Klein[1], S. Masson[1,2], C. Bouratzis[3], V. Grechnev[4], A. Hillaris[3], and P. Preka-Papadema[3]

[1] LESIA-UMR 8109, Observatoire de Paris, CNRS, Univ. Paris 6 & 7, Observatoire de Meudon, F-92195 Meudon, France; e-mail: ludwig.klein@obspm.fr
[2] Space Weather Laboratory, NASA-Goddard Space Flight Center, 8800 Greenbelt Road, Greenbelt, MD 20771, USA; e-mail: sophie.masson@nasa.gov
[3] Section of Astrophysics, Astronomy and Mechanics, Department of Physics, University of Athens, Zografos (Athens), GR-15783, Greece; e-mail: kbouratz@phys.uoa.gr
[4] Institute of Solar-Terrestrial Physics SB RAS, Lermontov St. 126A, Irkutsk 664033, Russia; e-mail: grechnev@iszf.irk.ru

Received ???, 2014; accepted ???

ABSTRACT

Context. The highest energies of solar energetic nucleons detected in space or through gamma-ray emission in the solar atmosphere are in the GeV range. Where and how the particles are accelerated is still controversial.
Aims. We search for observational evidence on the acceleration region(s) by comparing the timing of relativistic protons detected at Earth and radiative signatures in the solar atmosphere.
Methods. To this end a detailed comparison is undertaken of the double-peaked time profile of relativistic protons, derived from the worldwide network of neutron monitors during the large particle event of 2005 January 20, with UV imaging and radio petrography over a broad frequency band from the low corona to interplanetary space.
Results. We show that both relativistic proton releases to interplanetary space were accompanied by distinct episodes of energy release and electron acceleration in the corona traced by the radio emission and by brightenings of UV kernels in the low solar atmosphere. The timing of electromagnetic emissions and relativistic protons suggests that the first proton peak was related to the acceleration of gamma-ray emitting protons during the impulsive flare phase, as shown before. The second proton peak occurred together with signatures of magnetic restructuring in the corona after the CME passage.
Conclusions. We attribute the acceleration to reconnection and possibly turbulence in large-scale coronal loops. While type II radio emission was observed in the high corona, there is no evidence of a temporal relationship with the relativistic proton acceleration.

Key words. Acceleration of particles – Sun: coronal mass ejections (CMEs) – Sun: flares – Sun: particle emission – Sun: radio radiation – Sun: solar-terrestrial relations

1. Introduction

On certain occasions transient energetic particle fluxes from the Sun, called solar energetic particle (SEP) events, may comprise relativistic nucleons at energies up to several GeV or even tens of GeV. Upon impinging on the Earth's atmosphere these particles trigger nuclear cascades that produce secondaries detectable by ground-based neutron monitors and muon telescopes. Therefore these particular SEP events are called Ground Level Enhancements (or Ground Level Events; GLEs). The rarity of GLEs - only 72 were detected since 1942, including a small event on 2014 Jan 06 - clearly shows that they are produced by extreme energies for a solar event. Understanding their origin is therefore one of the more challenging tasks in research on solar eruptive activity. A comprehensive summary of GLE observations was given by Lopate (2006). The historical text by Carmichael (1962) is still very informative.

GLEs are produced in conjunction with intense flares (Belov et al. 2010) and extremely fast coronal mass ejections (CMEs; Gopalswamy et al. 2005). The acceleration mechanisms are thought to be related to the flare, which generally means magnetic reconnection, or to the shock wave generated by the CME. Which of the flare or the shock wave actually is the accelerator is hard to say on observational grounds. Statistical associations do not provide an answer. The relative timing of particle arrival at the Earth with respect to manifestations of flares and CMEs has generally been used in a very simplified way, hypothesizing that when the release of the first relativistic particles observed could not be related to the *onset* of radiative signatures of energetic particles during a flare (gamma-ray, hard X-ray, radio), a flare-independent acceleration process had to be invoked. From this line of reasoning many studies concluded that relativistic solar particles were accelerated at CME shocks (Lockwood et al. 1990; Kahler 1994; McCracken et al. 2012). Others found a mixed contribution of impulsive flare-related and delayed acceleration processes (Aschwanden 2012). Since time-extended gamma-ray emission of relativistic protons was observed in some events, prolonged acceleration to relativistic energies must also occur in some flaring active regions (see Hudson & Ryan 1995; Ryan 2000; Chupp & Ryan 2009, and references therein). Recent FERMI observations revealed that gamma-ray emission from relativistic protons may persist over hours in the flaring active region (Ackermann et al. 2014; Ajello et al. 2014).

Difficulties to relate SEP time histories to dynamical processes in the solar atmosphere arise because by the time the particles reach 1 AU their profile has been distorted by interplanetary propagation. GLEs often occur in periods of high activity, when the interplanetary space has a transient magnetic

structure due to CMEs, which introduce uncertainties about the path taken by the particles (Masson et al. 2012). Detailed timing studies exploring the relationship between GLEs and their parent solar activity are therefore still rare. The GLE of 2005 Jan 20 is a particularly favourable case, because it displayed a well-defined rapidly rising time profile at the beginning and a distinct second rise a few minutes later. Evidence that the first release was related to particle acceleration in the flaring active region in the low corona was brought by different publications (e.g. Simnett 2006, 2007; Kuznetsov et al. 2008; Grechnev et al. 2008; McCracken et al. 2008; Masson et al. 2009). In the present paper we pursue the investigation of Masson et al. (2009)[1] through a more detailed comparison between the two rises of the relativistic proton time profile derived from neutron monitor measurements with high-quality radio and UV observations.

This article is structured as follows: Section 2 introduces the observations (2.1), describes the time profile of relativistic protons detected at Earth (2.2) and gives an overall comparison with radio observations (2.3). It is concluded that two successive proton releases at the Sun can be identified in the GLE observation. The first is discussed briefly (Sect. 2.3.1) with reference to *paper 1* and to the evolution of the dm-m-wave dynamic spectrum studied by Bouratzis et al. (2010). A more detailed analysis of the radio emission accompanying the second relativistic proton release (Sect. 2.3.2) leads us to suggest that the particles are accelerated during dynamical processes in the magnetically stressed corona after the CME passage (2.3.3). The findings are summarised in Sect. 2.4 and discussed in Sect. 3 with respect to previous work on the origin of relativistic solar nucleons.

2. Relativistic proton releases and electromagnetic emission during the 2005 Jan 20 flare and CME

2.1. Observations

Relativistic protons penetrating into the Earth's atmosphere are observed by the worldwide network of neutron monitors. Since individual neutron monitors detect signals from protons with different arrival directions and different low-energy limits, depending on the instrument's location within the Earth's magnetic field, the observations of the network can be inverted using a fitting procedure, and parameters of the energy spectrum (actually the rigidity spectrum) and the angular distribution of the arriving protons can be derived. This was done by Bütikofer et al. (2006), using a power-law spectrum in magnetic rigidity. The results are also described in *paper 1*. Time histories of the proton intensities at rigidities of 2 and 5 GV, corresponding respectively to kinetic energies of 1.27 and 4.15 GeV, are displayed in the top panel of Fig. 1 (Fig. 1.e).

In order to elucidate the acceleration processes we compare the relativistic proton time profiles with electromagnetic tracers of energy release, electron acceleration and electron propagation from the corona to 1 AU. Whole Sun records in the X-ray and radio band are shown in the lower panels of Fig. 1:

a) Soft X-ray (SXR) fluxes (Fig. 1.a) are monitored by the *Geostationary Operational Environmental Satellites* (GOES) operated by NOAA[2]. The emission comes from plasma heated during the flare and traces the history of thermal energy input and loss in the flaring active region.
b) Flux density time profiles at selected radio frequencies (Fig. 1.b) were observed by the *Radio Solar Telescope Network* (RSTN; 0.245-15.4 GHz range) of the US Air Force[3] and by the Radio Polarimeters of the Nobeyama

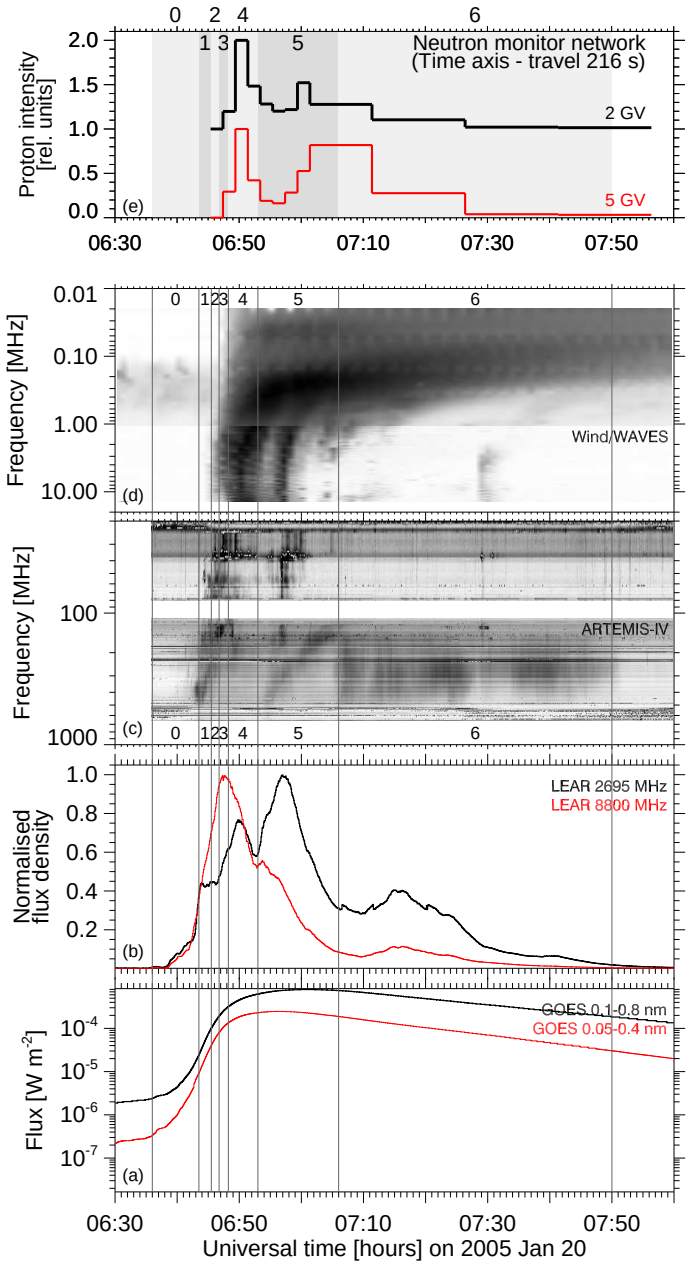

Fig. 1. X-ray and radio emission and the relativistic proton profile of the 2005 Jan 20 event. From bottom to top: (a) soft X-rays $\lambda = 0.1 - 0.8$ nm (dark line) and 0.05-0.4 nm (light; red in the colour plot of the online version); (b) microwaves (dark line 2.7 GHz, light - red in the colour display - 8.8 GHz; RSTN network, Learmonth); (c) dynamic radio spectrum at dm-m waves (ARTEMIS-IV; inverse colour scale; 1 s integration time); (d) decametre-kilometre wave radio emission (Wind/WAVES; inverse colour scale); (e) proton flux time history at 2 GV (dark curve) and 5 GV (light curve; red in the online version) rigidity (kinetic energy 1.27 and 4.15 GeV, respectivelyy), time axis shifted back by 216 s. The intervals delimited by vertical lines and numbered 0 to 6 are different episodes of particle acceleration, as discussed in the text.

[1] Masson et al. (2009) will be cited as *paper 1* in the following.
[2] http://www.ngdc.noaa.gov/stp/SOLAR/
[3] provided by NGDC/WDC Boulder http://www.ngdc.noaa.gov/stp/space-weather/solar-data/solar-f

Radio Observatory (NoRP; 1.0-80 GHz; Nakajima et al. 1985)[4]. Microwaves ($\nu \geq 1$ GHz) are due to the gyrosynchrotron process of near-relativistic electrons (energies between about 100 keV and a few MeV) with an admixture of collective plasma emission near the electron plasma frequency or its harmonic in the range up to a few GHz. Microwave emission comes from low coronal heights, a few ten thousands of kms above the photosphere.

c) Decimetre-to-metre wave dynamic spectrograms (Fig. 1.c) are observed by the ARTEMIS IV[5] solar radio spectrograph at Thermopylae (Greece; Caroubalos et al. 2001; Kontogeorgos et al. 2006, 2008). It consists of a 7-m parabolic antenna covering the dm-m wave range, to which a dipole antenna was added recently in order to cover the long metre-decametre wave range. Two receivers operate in parallel, a sweep frequency analyzer (ASG) covering the 650-20 MHz range in 630 data channels with a cadence of 10 samples/sec and a high sensitivity multi-channel acousto-optical analyzer (SAO), which covers the 270-450 MHz range in 128 channels with a high time resolution of 100 samples/sec. The radio waves are predominantly plasma emission which, given the frequency range, occurs in a range between about 0.1 and 1 $R_\odot$ above the photosphere.

d) Dynamic spectra at decametric-to kilometric waves (14 MHz to some tens of kHz; Fig. 1.d) are obtained from the WAVES spectrograph aboard the Wind spacecraft (Bougeret et al. 1995). The radio waves are plasma emissions from the high solar corona, about 2 to 3 $R_\odot$ above the photosphere near 10 MHz, to 1 AU (~20 kHz).

The ordering of the panels in Fig. 1 hence reflects a tracing of energy release and electron acceleration in the low corona (SXR and microwaves) to electrons in the interplanetary medium near 1 AU (radio waves at a few tens of kHz). The reader is referred to the reviews of Bastian et al. (1998) and Nindos et al. (2008), and references therein, for a more detailed presentation of radio emission processes.

2.2. Time profile of relativistic protons detected at Earth

The top panel of Fig. 1 shows the intensity-time history of relativistic protons after subtraction of a travel time of 216 s evaluated in *paper 1*, and which will be justified below. A remarkable feature of the time profile is its double-peaked structure, As shown in *paper 1* (Fig. 1) the first peak was nearly exclusively due to anti-sunward streaming protons, while during the second peak anti-sunward streaming protons were observed on top of an isotropic population. McCracken et al. (2008) inferred the double-peak structure and the anisotropy characteristics from a semi-quantitative analysis of count rate time histories of the neutron monitor network. Plainaki et al. (2007) and Bombardieri et al. (2008) failed to detect the gap between the first and second pulse, because it was smeared out in their 5 min integrated data. However, the latter authors showed (their Fig. 5) that anisotropy was significant throughout the time interval of the second pulse, although much weaker than during the first.

The question whether the second rise of the proton profile is a signature of a second solar particle release or not is debated in the literature. Particle reflection at magnetic bottlenecks beyond 1 AU due to previous CMEs, or magnetic mirroring in an extended loop has been discussed in some other GLEs (Bieber et al. 2002; Sáiz et al. 2008), and was also proposed for the 2005 Jan 20 event[6]. But since the second pulse is due to anti-sunward streaming protons, its timing cannot be explained by reflection of particles from the first release. For one would have to require that the reflected particles travel back to the Sun and are again reflected earthward. Even if such a process could create a new rise, the time needed for the particles to travel sunward from the bottleneck and again earthward is too long: from the estimated travel time of 12.5 min between the Sun and the Earth in the first pulse (see below), to which the travel time between the Earth and the bottleneck and back to the Earth must be added, the protons would need more than 25 min after the first pulse to reach the Earth a second time. But the second rise starts only about 12 min after the first. This suggests that the second rise of the proton time profile is indeed due to a second release of relativistic protons from the Sun. When detected at Earth, the particles from this release are, however, superposed on a strong background, to which reflection at a magnetic barrier beyond 1 AU may well have contributed. Because of this background the second release had lower intensity than the first.

In summary we consider that the two pulses in the relativistic proton time profile result from separate acceleration processes near the Sun. The actual time profile of the second pulse depends strongly on the fitted parameters of the rigidity spectrum. This is seen by the comparison of the time profiles at different proton energies in Fig. 1.e, where the profile at 2 GV has an impulsive peak at the onset of the long second pulse seen at 5 GV. In the following comparisons the existence of the new release is considered as established, while the duration is considered uncertain.

Table 1. Acceleration episodes during the 2005 Jan 20 event.

Episode	EM emission	GLE signature
0	Early SXR rise; cm-dm-λ, no m-km-λ emission	none observed
1	SXR, HXR, cm-m-λ rise, no Dm-km-λ emission	none observed
2-4	SXR rise; π-decay γ, main HXR, cm-λ, dm-km-λ (IV, III)	1st peak
5	SXR peak and early decay, HXR and mm-short cm-λ decay, further long cm-km-λ (IV, III)	2nd peak
6	SXR decay, further cm-λ peaks, m-λ IV, DH$^{(a)}$ II, isolated DH III	decay 2nd peak

(a)

"DH" means dekametric-hectometric.

2.3. Comparison of the proton time profile with radio, X-ray and UV emission

The SXR time profile of the event (Fig. 1.a) had a smooth rise and fall, while the electromagnetic emission evolved in distinct steps that allow us to roughly distinguish different acceleration episodes. They are labelled from 0 to 6 in Fig. 1 and are summarised in Table 1. The hard X-ray (HXR) emission is not shown in Fig. 1. Its overall evolution was similar to the 8.8 GHz microwaves. Details are given in Fig. 2 of *paper 1*. The radio emission started increasingly later with decreasing frequency: episode 0 during the early rise of the SXR burst comprised cm-

[4] http://solar.nro.nao.ac.jp/

[5] *Appareil de Routine pour le Traitement et l'Enregistrement Magnétique de l' Information Spectrale*, http://web.cc.uoa.gr/~artemis/

[6] see Abstract in Ruffolo et al. (2010)

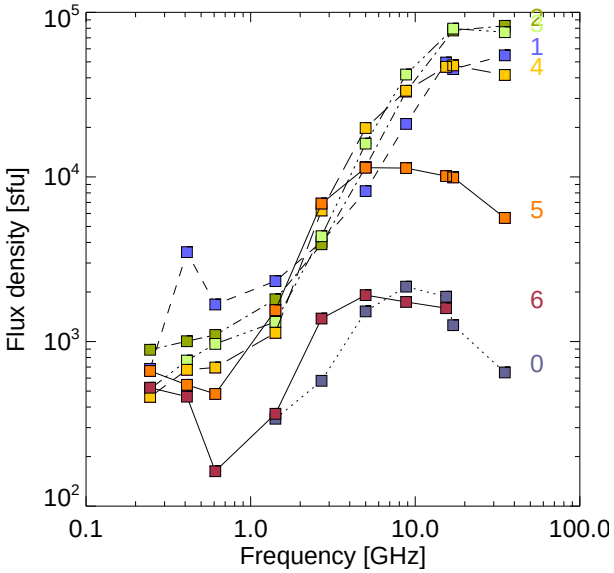

Fig. 2. Whole Sun radio spectra during the different acceleration episodes, as indicated to the right of the curves. Each spectrum is an average over 1 min taken at the midpoint of the acceleration episode. Data compiled from the Learmonth and San Vito RSTN stations (0.245-15.4GHz) and the Nobeyama Radio Polarimeters (17 and 35 GHz). The flux density (ordinate) is given in solar flux units (1 sfu= 10^{-22} W m^{-2} Hz^{-1}.

mm wave gyro-synchrotron emission since 06:36 UT, as shown by the flux density spectrum labelled "0" in Fig. 2 (dotted curve). This emission had no counterpart at metric and longer waves (for details see Figs. 1-3 of Bouratzis et al. 2010). The low-frequency limit of the radio burst drifted gradually towards lower frequencies. This well-defined low-frequency cutoff and the absence of type III burst emission suggest that the electron acceleration proceeded in low-lying coronal structures and that the electrons remained confined there during episode 0. The gradual progression towards lower frequencies shows that the confining magnetic structures were evolving or that the acceleration region comprised successively more extended structures.

2.3.1. Solar phenomena associated with the first proton release

The brightest impulsive phase emission was observed at gamma-ray, HXR and microwave wavelengths during episodes 1 to 4. This is illustrated by the 8.8 GHz time profile in Fig. 1.b. As discussed in *paper 1*, gamma-ray emission of relativistic protons, produced by pion decay, was first observed in episode 2. The sudden appearance of type III bursts in the WAVES spectrum at this time (Fig. 1.d) demonstrates that electron beams were released to the interplanetary space. If we hypothesize that the first release of protons producing the GLE started at this time, too, their intensity profile must be shifted back by a travel time of 216 s, as done in Fig. 1.e. This travel time to the Earth implies an interplanetary path length near 1.4-1.5 AU (see Sect. 3.1 of *paper 1*), which is longer than the nominal Parker spiral length. Since the interplanetary medium had been strongly disturbed by CMEs ejected at previous days, a longer path length than predicted by Parker's model is plausible (Masson et al. 2012). The time lapse between the first acceleration signatures seen in microwaves (06:36 UT) and the first escape of particles to interplanetary space was 9-10 minutes.

Although the 2005 Jan 20 event was clearly eruptive, with a fast CME, dimmings and signatures of EUV waves (Grechnev et al. 2008), the ARTEMIS IV spectrum showed no evidence of a classical drifting metre wave type II burst during episodes 0 to 4. Short features with type II-like drifts were discussed by Bouratzis et al. (2010), but their identification as shock signatures is ambiguous because characteristic type II fine structures such as band splitting and fundamental-harmonic structure were absent.

2.3.2. Solar phenomena associated with the second proton release

The relative timing of relativistic protons at Earth and radio emissions derived for the first peak also determines the relative timing during the second peak. As seen in Fig. 1.d, the rise to this second peak was accompanied by a new group of decametric-to-hectometric (DH) type III bursts. The release of electron beams to the high corona and interplanetary space at this specific time strengthens the conclusion that the second rise of the relativistic proton profile was due to a new solar particle release. A new episode of near-relativistic electron acceleration is also seen as a minor peak superposed on the decaying 8.8 GHz time profile in Fig. 1.b, and as a clear new peak at 2.7 GHz. Based on these time profiles, we identify new acceleration episodes 5, including the onset of the second proton peak, and 6 for later acceleration that produced weaker new peaks at microwave frequencies.

The whole Sun radio spectra derived from the fixed-frequency observations during the seven acceleration episodes (Fig. 2) have a typical gyro-synchrotron shape. The Nobeyama flux density at 3.75 GHz, which is not shown in this plot, was about twice as high as at neighbouring RSTN frequencies. But the spectral shape was similar as in the RSTN observations, with a positive slope between ~1 GHz and a peak frequency near 30 GHz in the impulse phase (episodes 1 to 4). Optically thick emission up to 30 GHz is consistent with intense magnetic fields close to sunspots, where the optical and UV ribbons were observed during the impulsive phase (Grechnev et al. 2008). These authors evaluated a magnetic field strength of 1600 G. The spectra still have the gyro-synchrotron shape in episodes 5 and 6, but with a much lower peak frequency near 5 GHz. This indicates radiation from a source with much weaker magnetic field than in the impulsive phase. The gyro-synchrotron spectra extend down to 610 MHz and perhaps lower, as suggested by the uniform grey background in the dm-m wave spectrum (Fig. 1.c). This shows that near-relativistic electrons accelerated during episodes 5 and 6 were released into magnetic structures within an extended height range in the corona.

Superposed on the gyro-synchrotron emission during episode 5 is a band of emission at dm-m wavelengths that crosses the frequency range 650-100 MHz in Fig. 1.c. A more detailed view is shown in Fig. 3. The emission undergoes a systematic drift from high (06:55 UT near 500 MHz) to low frequencies (~07:02 UT near 150 MHz). It is accompanied on its low-frequency side (especially 20-80 MHz, around 06:57 UT) by radio emissions that connect to the type III burst below 14 MHz, indicating that electrons got access to interplanetary space at least during the early part of episode5.

A clear new episode of energy release starting near 06:54 UT can also be seen in UV observations during episode 5, and the sources can be localised in flare kernels at 160 nm wavelength with the *Transition Region and Coronal Explorer* (TRACE; Handy et al. 1999). An average image of the flaring active region was computed using 20 snapshots between 06:52:41 and

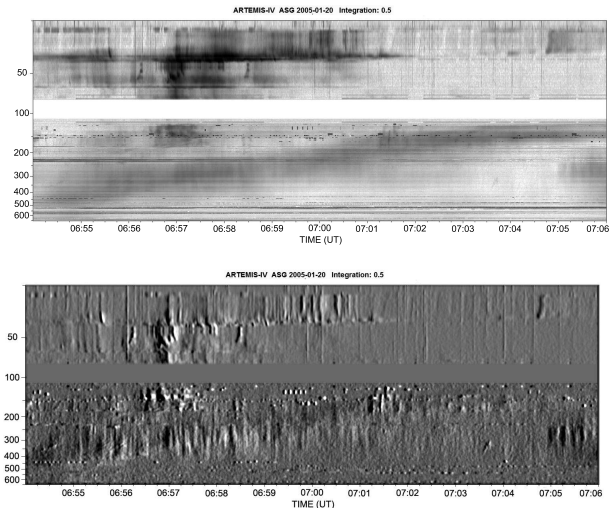

Fig. 3. Detail of the dynamic spectrum (ARTEMIS IV; top; inverse grey-level scale) and differential spectrum (bottom) during the narrowband drifting lane in episode 5. The vertical axis gives the frequency in MHz. The series of dark spots near the low-frequency border of the total flux density spectrum is an instrumental artefact.

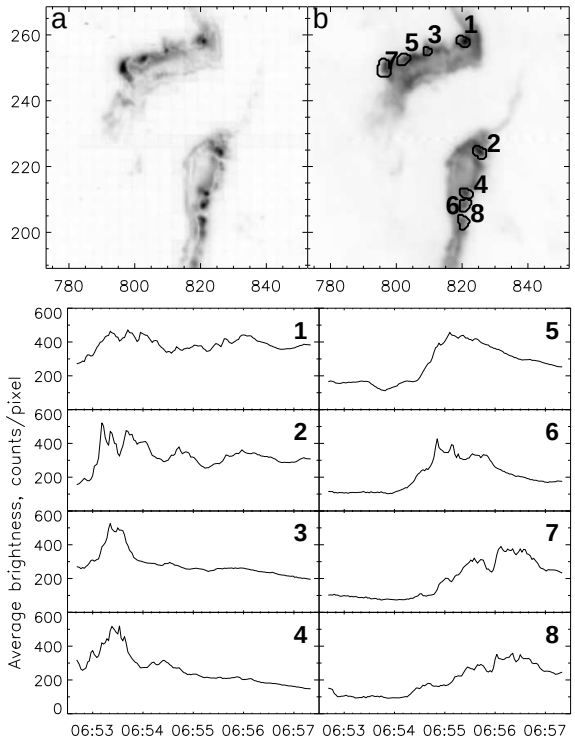

Fig. 4. Flare ribbons and flare kernels (TRACE 160 nm) during the impulsive and early post-impulsive phase of the 2005 Jan 20 flare. *Top*: maps of the variance of the emission (a) showing the flare kernels and of the average emission (b), showing the flare ribbons, with overlaid flare kernels as identified in the variance map (50% contour; see text). *Bottom*: time profiles of the individual kernels, numbered as in map (b). Odd-numbered kernels are in the northern ribbon, even-numbered ones in the southern ribbon. Successive odd and even numbers denote conjugate kernels.

06:57:30 UT, together with a map of the variance (see Grechnev 2003) of the brightness time history. The variance map in the top left panel of Fig. 4 shows the most variable emission in the flare kernels. The 50% contours of the variance map are overlaid on the average image, which displays the flare ribbons, in the top right panel. The individual light curves in the bottom panels of Fig. 4 display the time histories of brightness in the kernels labelled 1 to 8. Successive pairs show similar light curves from opposite flare ribbons. Their similarity suggests that the kernels are conjugate footpoints of flaring loops. Of particular interest for our present discussion are the light curves of kernels (5, 6) and (7, 8), because they show a clear activation at 6:54 UT. These kernels were located on the outer sides of the average flare ribbons, respectively at the eastern and southern extremes of the northern and southern ribbon. They show that a new episode of energy release started at 06:54 UT, together with the new microwave peak and the drifting band of dm-m wave radio emission. The energy release starting 06:54 UT hence involved part of the structures that brightened in the impulsive phase (kernels 1, 2) and newly brightening kernels that probably relate to more extended coronal magnetic structures than the previous episodes. The first post flare loops became visible between the flare ribbons in TRACE UV images at about 7:04 UT, well after the brightening of these flare kernels, and persisted throughout the day (Grechnev et al. 2008). The kernels hence signal a distinct early energy release process during episode 5, but the subsequent appearance of post flare loops suggests that energy release continued at increasing coronal height.

The nature of the slowly drifting band of radio emission in the 500-100 MHz range (Fig. 3) can give hints to the electron acceleration process during episode 5 and, because of the common timing, possibly also on the acceleration of relativistic protons. Because of its drift rate and relative bandwidth this feature was identified as a type II burst in several publications (Pohjolainen et al. 2007; Masson et al. 2009). It was recognised by Pohjolainen et al. (2007) that given the frequency range, which is expected to be emitted within a solar radius above the photosphere, this burst could not be emitted at the front of the CME that was seen at heliocentric distance 4.5 $R_\odot$ by SoHO/LASCO at 06:54 UT. But it could be due to a shock driven by the lateral expansion of the CME (see, for instance, the coronal shock shape in the simulations of Pomoell et al. 2008).

However, a more detailed analysis of the ARTEMIS IV radio spectrum shows that this radio emission is not a type II burst. The total and differential dynamic spectrograms of the drifting lane in Fig. 3 show a drift rate of about -0.8 MHz s^{-1} (relative drift rate -0.0026 s^{-1}) and an instantaneous bandwidth of about 30% of its centre frequency. While these values are typical of type II bursts at these frequencies (Mann et al. 1995), the spectrum is basically a continuum with different types of fine structure during different time intervals. None of the fine structures that are common in type II bursts are seen, such as fundamental/harmonic structure, splitting of the band into narrow lanes, or short bursts with rapid frequency drift called herringbone bursts (Nelson & Melrose 1985; Nindos et al. 2008).

The most prominent fine structures of the drifting lane, which stand out in the differential spectrum (Fig. 3, bottom), are broadband pulsations. A detailed spectrum of the early phase is shown in Fig. 5, using the high spectral resolution mode of the ARTEMIS IV acousto-optical receiver (SAO). The high-resolution spectra were high-pass filtered along the time axis to suppress both the continuum background and the terrestrial emitters, which manifest themselves as narrow lines parallel to the time axis (see, for instance, the upper panel of Fig. 3). Then we separated fibers and spikes from pulsations using high-pass

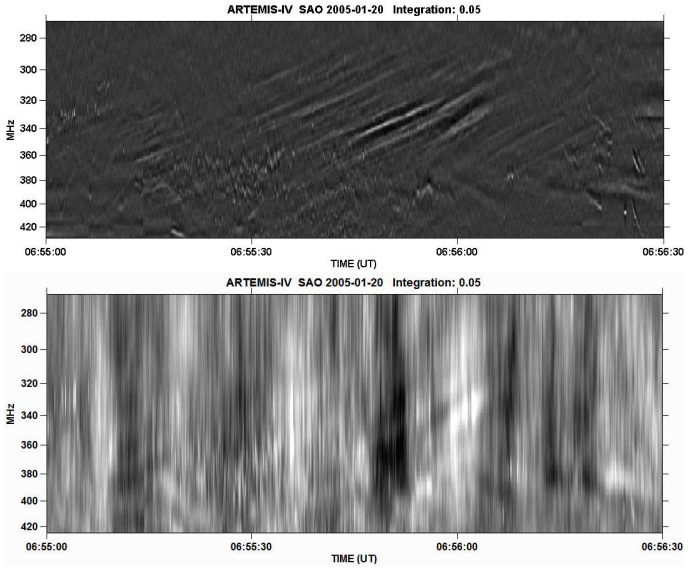

Fig. 5. Details of the dynamic spectrum of the drifting continuum in Fig. 3 with high spectral resolution: fiber bursts and narrow-band spikes (top), broadband pulsations (bottom).

filtering along the frequency axis to eliminate pulsations (Fig. 5, upper panel) and low-pass filtering to suppress fiber bursts and spikes (Fig. 5, lower panel). Besides the pulsations, the drifting emission feature hence also shows narrow-band spikes above about 340 MHz and fiber bursts with negative frequency drift on their low-frequency side. Chernov (2011) gave an extended review of fine structures in solar radio bursts. It is clear from these spectral observations that the slowly drifting lane of dm-m wave emission that accompanied the second relativistic proton release was a burst of type IV, also called a flare continuum. This gives a clue to the acceleration process, as will be discussed in Sect. 2.3.3.

The dynamic radio spectrum below 14 MHz (Fig. 1.d) shows a type II burst at its high-frequency border near the start of episode 6. This burst was labelled II(3) in Bouratzis et al. (2010). It was not the low-frequency extension of a metre wave type II burst - at least no corresponding signature is seen in Fig. 1.c. This suggests that the shock-related radio emission truly started near the end or after episode 5. It followed in time the drifting type IV burst, and may well be related to the expanding CME structures of which the type IV source is part. There is no time correspondence between the type II burst and the start of the second relativistic proton peak.

2.3.3. An interpretation of particle acceleration during the second relativistic proton release

Here we attempt an interpretation of the observations during episode 5, related in particular to the origin of the drifting type IV burst. Although we have no imaging observations of the dm-m wave radio sources on 2005 Jan 20, we can refer to well-observed events reported in the literature where a consistent scenario of radio emission during the formation and outward expansion of a flux rope has been developed. The imaging observations typically show the presence of an outward moving outer source and one or more sources at lower altitude with or without systematic motion (Laitinen et al. 2000; Klein & Mouradian 2002; Vršnak et al. 2003; Pick et al. 2005; Maia et al. 2007; Huang et al. 2011; Démoulin et al. 2012). Within a classical scenario of flux rope formation, as described by Démoulin et al. (2012), the outward moving radio source is ascribed to electrons accelerated during reconnection in the underlying current sheet, from where they are injected upward onto freshly reconnected field lines that are draped around the flux rope. Since the flux rope moves outward and expands, the internal electron density decreases, and the plasma emission of the confined electrons occurs at gradually decreasing frequencies, as observed in the type IV continuum during episode 5. Electrons injected downward from the current sheet generate emission in newly reconnected underlying loops. The near-relativistic part of this population could explain the gyro-synchrotron spectrum with peak frequency near 5 GHz (Fig. 2). Gyro-synchrotron emission from electrons in the overlying flux rope was also reported in other events (Bastian et al. 2001; Maia et al. 2007), but it can only be detected with imaging observations.

Electron acceleration in the current sheet underneath a CME is in line with other observations: Aurass et al. (2009) compared spectral observations of a type IV burst having a similar spectrum as on 2005 Jan 20 with white-light and spectroscopic UV observations. They concluded that the radio emission came from the current sheet behind a CME. Benz et al. (2011) showed evidence from the spatial organisation of the sources of two pulsating continua with the region above coronal hard X-ray sources, suggesting again the current sheet of the standard eruptive flare scenario as the acceleration region. Kliem et al. (2000) presented spectrographic observations of another drifting and pulsating source, which occurred together with the ejection of a soft X-ray plasmoid. They concluded from a comparison with numerical simulations that a current sheet underwent repeated reconnection, tearing and coalescence of magnetic islands, leading to repeated bursts of particle acceleration during the gradual build-up of the plasmoid that was eventually ejected

The dm-m-wave radio emission during episode 5 on 2005 Jan 20 and its simultaneity with the start of the second release of relativistic protons hence suggests that both radio emitting electrons and relativistic protons were accelerated during the dynamical evolution of coronal magnetic fields in the aftermath of a CME. The scenario involves closed magnetic field lines and does not explain the particle escape to the interplanetary space. But radio emission was also detected at the low-frequency side of the type IV burst near the start of episode 5 (around 06:57 UT, 30-150 MHz in Fig. 3). It had complex spectral structure, as shown in the difference spectrum in the lower panel, with many narrow-band bursts. This was hence not a type III burst, but at still lower frequencies WAVES did see a new type III burst (Fig. 1.d). It is tempting to interpret the spectral fine structure in the 30-150 MHz range as an indication of magnetic reconnection between the CME and ambient open magnetic field lines (see also Démoulin et al. 2012). This would allow the relativistic protons to escape as required for the interpretation of the GLE. Such a particle release scenario was modelled by Masson et al. (2013).

We note that the scenario of particle acceleration in the corona behind the CME does not imply that SEP events are always produced after the CME passage. Kahler et al. (2000) reported that events of arcade formation observed in SXR are usually not accompanied by SEP events. As stated in Sect. 2.3.2, the observed signatures of arcade formation on 2005 Jan 20 started only at the end of acceleration episode 5. There must be supplementary requirements that ought to be fulfilled in order to accelerate relativistic protons in this situation, perhaps related to the general energetics of the flaring active region or the CME.

2.4. Summary of results

Particle acceleration during the 2005 Jan 20 flare/CME event comprised several successive parts with different responses in different particle populations:

1. The relativistic proton event observed at Earth (GLE) revealed two distinct solar particle releases.
2. Each was associated with type III bursts showing the escape of subrelativistic electron beams to the interplanetary space.
3. The gamma-ray, hard X-ray and radio emissions showed that the event started with an impulsive phase consisting of several successive acceleration episodes. In one of the later episodes, about 9 min after the first signature in radio waves, relativistic protons were also accelerated (see *paper 1*).
4. During the same episode intense type III emission started at decametric and longer waves, showing that electrons had access to the high corona and interplanetary space at the time of the first relativistic proton acceleration shown by the gamma-rays.
5. The second relativistic proton release started near the peak of the SXR burst. It was again accompanied by a type III burst. A type IV burst was observed at dm-m wavelengths. It accompanied new microwave emission, which was more pronounced at frequencies of a few GHz rather than at the higher frequencies that dominated during the impulsive phase acceleration. A clear new energy release was seen in UV flare kernels, and was followed by the appearance of post flare loops. The radio emission is consistent with a scenario of electron acceleration in the stressed magnetic fields behind the CME, and by inference we suggest that the relativistic protons of the second pulse were also accelerated in this environment.
6. Type II emission was clearly seen at decametric waves ($\nu \leq$ 14 MHz), but started after the second proton peak. Despite the likely presence of shock waves in this very dynamic event, there is no time correspondence between their radio signatures and the timing of the acceleration and release of relativistic protons detected at Earth.

3. Discussion

3.1. Radio evidence on the evolution of particle acceleration and release in the 2005 Jan 20 GLE

Through its sensitivity to non thermal electrons and its relationship to the electron plasma frequency, radio emission provides valuable information on electron acceleration in different flare phases and on their release to the interplanetary space. This diagnostic has been applied here to the impulsive and post-impulsive phases of the 2005 Jan 20 flare-CME event. Common timing relationships suggest that this information has bearing on the acceleration and release of relativistic protons.

3.1.1. Impulsive phase acceleration - the first relativistic proton release

During the impulsive phase of the event several episodes of particle acceleration were identified, while the dm-m-wave radio emission extended to decreasing frequencies. During one of these episodes relativistic protons were first detected due to their production of pion-decay gamma-rays. The extension of the radio emission towards lower frequencies means that the electrons had access to successively more extended structures. Eventually they could escape to the interplanetary space, during the episode when the pion decay gamma-ray emission of relativistic protons was first seen. We note that while the radio emission comes from electrons and does not trace protons, the common timing with the pion-decay gamma-ray emission from interacting protons with similar energies as the GLE protons is a strong argument that the acceleration of the two populations was closely related (see Vilmer et al. 2003, and references therein for a more detailed discussion of pion decay gamma rays from relativistic protons). The access to space of relativistic protons from the flaring active region provides a convincing explanation of the first rise of the GLE. Similar successive increases of the spectral range of radio bursts were reported in other flares with strong particle acceleration (Trottet et al. 1998; Rieger et al. 1999). On occasion radio emission may remain cut off during the entire flare, indicating that the accelerated particles remain confined in the low corona (Klein et al. 2011). This is clearly not the case on 2005 Jan 20, but particles accelerated in the flaring active region only got access to space in the course of the impulsive phase evolution, not since its start.

The time delay between the first relativistic proton release and the first signature of impulsive electron acceleration (9 min) is significant and shows that typical delays of several minutes (Cliver et al. 1982; Aschwanden 2012) do not at all imply that interacting and escaping particles need different acceleration processes. Such delays are found here to result from the evolution of both the acceleration process(es) during the impulsive phase and the conditions for particle escape from the corona. McCracken et al. (2008) concluded that the relativistic protons of the first peak on 2005 Jan 20 remained confined during a few minutes before being released to interplanetary space. This conclusion was based (1) on a smoothed version of the gamma-ray time profile, from which the authors estimated too early a start of the emission and hence of the inferred acceleration of relativistic protons (see *paper 1*), and (2) on the hypothesis that the protons had to travel along a Parker spiral field line, whereas the interplanetary medium was strongly disturbed by previous CMEs (Masson et al. 2012). Therefore we conclude on a direct release of the protons producing the first peak of the GLE in the course of the impulsive phase of the associated flare.

3.1.2. Post-impulsive phase acceleration - the second relativistic proton release

Electron acceleration during this event clearly proceeded well beyond the impulsive phase, as shown by the long lasting radio emission. During the second release of relativistic protons, which started near the maximum of the soft X-ray burst, the hard X-ray and high-frequency (≥8 GHz) microwave emissions were decaying and showed only a minor new peak. But clear rises of emission were found in microwaves and at dm-m waves, as well as in UV kernels at the periphery of the flare ribbons. This is consistent with a new phase of energy release and particle acceleration, likely in a more tenuous plasma than before. From the properties of the radio emission we argued that a plausible environment of the acceleration was the post-CME corona with a reconnecting current sheet. Time-extended acceleration of relativistic protons was discussed with respect to long duration gamma-ray bursts by Ryan (2000) and Chupp & Ryan (2009). Among the mechanisms invoked are direct electric field acceleration in the reconnecting current sheet behind a CME and stochastic acceleration in large-scale turbulent loops (see also Vashenyuk et al. 2006). Both are consistent with the association between the proton acceleration and type IV radio emission, which shows the presence of large-scale loops in the aftermath of a CME. These scenarios show that the CME may be essential for the relativistic

proton acceleration even if the acceleration does not occur at a shock wave.

3.2. Comparison with other GLEs

The SEP event on 2005 Jan 20 illustrates the long-standing idea that GLEs may have a double-peaked structure, with an initial fast anisotropic particle population - called the 'prompt component' - followed by a more gradual and less anisotropic 'delayed component' (see review in Miroshnichenko 2001, chap. 7.3). McCracken et al. (2012) concluded that the sequence of an anisotropic impulsive peak and a less anisotropic gradual peak occurring 7-15 min later is a common occurrence when the parent active region is well connected to the Earth, while the absence of the impulsive peak is typical of poorly connected activity near or east of the central meridian or well beyond the western limb. One thus expects to see the first peak of the double-peaked structure on 2005 Jan 20 because of the favorable connection, while the second peak would be visible in all GLEs.

This is consistent with some earlier analyses of relativistic SEP release in temporal association with a type IV burst: in the event 2000 Jul 14 (W 07°; Klein et al. 2001a) the GLE was accompanied by a type IV burst with a spectrum that drifted slowly towards lower frequencies (see the radio spectrum in Klein et al. 2001b). Both the radio spectrum and the relativistic proton timing were similar to episode 5 of the 2005 Jan 20 event. The timing of the solar release of the first relativistic protons seen at Earth during the 1989 Sep 29 GLE (flare behind the western limb) was also found to be more consistent with a type IV burst than with the previous impulsive microwave burst (Klein et al. 1999). In these events we found that the early rise of the GLE was delayed by 10–20 min with respect to the first radiative signatures of electron acceleration in the impulsive phase. Both events were poorly connected. The association of the relativistic proton release with type IV emission suggests that in both a first anisotropic proton pulse was missed, in agreement with the McCracken et al. (2012) scenario.

Our results on 2005 Jan 20 are hence consistent with the basic scheme of successive relativistic particle releases during a GLE devised by (Miroshnichenko 2001, and references therein), McCracken et al. (2008) and McCracken et al. (2012). But they also emphasise that the solar acceleration history is not adequately described by a single impulsive phase acceleration process and a subsequent coronal acceleration by the CME shock.

Acknowledgements. The authors are grateful to K. Shibasaki (Nobeyama Radio Observatory), R. Bütikofer and E. Flückiger (University of Berne) and V. Kurt (Skobeltsyn Institute of Nuclear Physics, Lomonosov Moscow State University) for providing data. KLK acknowledges helpful discussions with J. Bieber, R. Bütikofer, P. Evenson, E. Flückiger, D. Lario, V. Petrosian and J. Ryan, and the kind hospitality of the solar radio astronomy group of the University of Athens and of the space research group of the National Observatory of Athens. This work was supported in part by the University of Athens Research Center (ELKE/EKPA), by the French Polar Institute (IPEV) and the French space agency (CNES).

References

Ackermann, M., Ajello, M., & Albert, A. *et al.*. 2014, ApJ, submitted
Ajello, M., Albert, A., & Allafort, A. *et al.*. 2014, ApJ, submitted
Aschwanden, M. J. 2012, Space Sci. Rev., 171, 3
Aurass, H., Landini, F., & Poletto, G. 2009, A&A, 506, 901
Bastian, T. S., Benz, A. O., & Gary, D. E. 1998, ARA&A, 36, 131
Bastian, T. S., Pick, M., Kerdraon, A., Maia, D., & Vourlidas, A. 2001, ApJ, 558, L65
Belov, A. V., Eroshenko, E. A., Kryakunova, O. N., Kurt, V. G., & Yanke, V. G. 2010, Geomagnetism and Aeronomy/Geomagnetizm i Aeronomiia, 50, 21
Benz, A. O., Battaglia, M., & Vilmer, N. 2011, Sol. Phys., 273, 363
Bieber, J. W., Dröge, W., Evenson, P. A., et al. 2002, ApJ, 567, 622
Bombardieri, D. J., Duldig, M. L., Humble, J. E., & Michael, K. J. 2008, ApJ, 682, 1315
Bougeret, J.-L., Kaiser, M. L., Kellogg, P. J., et al. 1995, Space Sci. Rev., 71, 231
Bouratzis, C., Preka-Papadema, P., Hillaris, A., et al. 2010, Sol. Phys., 267, 343
Bütikofer, R., Flückiger, E. O., Desorgher, L., & Moser, M. R. 2006, in 20-th European Cosmic Ray Symposium, http://www.lip.pt/events/2006/ecrs/proc/
Carmichael, H. 1962, Space Sci. Rev., 1, 28
Caroubalos, C., Maroulis, D., Patavalis, N., et al. 2001, Experimental Astronomy, 11, 23
Chernov, G. P., ed. 2011, Astrophysics and Space Science Library, Vol. 375, Fine Structure of Solar Radio Bursts
Chupp, E. L. & Ryan, J. M. 2009, Research in Astronomy, 9, 11
Cliver, E. W., Kahler, S. W., Shea, M. A., & Smart, D. F. 1982, ApJ, 260, 362
Démoulin, P., Vourlidas, A., Pick, M., & Bouteille, A. 2012, ApJ, 750, 147
Gopalswamy, N., Xie, H., Yashiro, S., & Usoskin, I. 2005, in International Cosmic Ray Conference, Vol. 1, 169–172
Grechnev, V. V. 2003, Sol. Phys., 213, 103
Grechnev, V. V., Kurt, V. G., Chertok, I. M., et al. 2008, Sol. Phys., 252, 149
Handy, B. N., Acton, L. W., Kankelborg, C. C., et al. 1999, Sol. Phys., 187, 229
Huang, J., Démoulin, P., Pick, M., et al. 2011, ApJ, 729, 107
Hudson, H. & Ryan, J. 1995, ARA&A, 33, 239
Kahler, S. 1994, ApJ, 428, 837
Kahler, S. W., McAllister, A. H., & Cane, H. V. 2000, ApJ, 533, 1063
Klein, K.-L., Chupp, E. L., Trottet, G., et al. 1999, A&A, 348, 271
Klein, K.-L. & Mouradian, Z. 2002, A&A, 381, 683
Klein, K.-L., Trottet, G., Lantos, P., & Delaboudinière, J.-P. 2001a, A&A, 373, 1073
Klein, K.-L., Trottet, G., Lantos, P., & Delaboudinière, J.-P. 2001b, A&A, 377, 687
Klein, K.-L., Trottet, G., Samwel, S., & Malandraki, O. 2011, Sol. Phys., 269, 309
Kliem, B., Karlický, M., & Benz, A. O. 2000, A&A, 360, 715
Kontogeorgos, A., Tsitsipis, P., Caroubalos, C., et al. 2008, Measurement, 41, 251
Kontogeorgos, A., Tsitsipis, P., Caroubalos, C., et al. 2006, Experimental Astronomy, 21, 41
Kuznetsov, S. N., Kurt, V. G., Yushkov, B. Y., & Kudela, K. 2008, in 30th International Cosmic Ray Conference, ed. R. Caballero, J. C. D'Olivo, G. Medina-Tanco, L. Nellen, F. A. Sánchez, & J. F. Valdés-Galicia, Vol. 1, 121–124
Laitinen, T., Klein, K.-L., Kocharov, L., et al. 2000, A&A, 360, 729
Lockwood, J. A., Debrunner, H., & Flueckiger, E. O. 1990, J. Geophys. Res., 95, 4187
Lopate, C. 2006, in AGU Monograph, Vol. 165, Solar Eruptions and Energetic Particles, ed. N. Gopalswamy, R. Mewaldt, & Torsti, J. (Washington DC: American Geophysical Union), 283–296
Maia, D. J. F., Gama, R., Mercier, C., et al. 2007, ApJ, 660, 874
Mann, G., Classen, T., & Aurass, H. 1995, A&A, 295, 775
Masson, S., Antiochos, S. K., & DeVore, C. R. 2013, ApJ, 771, 82
Masson, S., Démoulin, P., Dasso, S., & Klein, K.-L. 2012, A&A, 538, A32
Masson, S., Klein, K.-L., Bütikofer, R., et al. 2009, Sol. Phys., 257, 305
McCracken, K. G., Moraal, H., & Shea, M. A. 2012, ApJ, 761, 101
McCracken, K. G., Moraal, H., & Stoker, P. H. 2008, J. Geophys. Res., 113, 12101
Miroshnichenko, L. I. 2001, Solar Cosmic Rays (Dordrecht/Boston/London: Kluwer Acad. Publ.)
Nakajima, H., Sekiguchi, H., Sawa, M., Kai, K., & Kawashima, S. 1985, PASJ, 37, 163
Nelson, G. J. & Melrose, D. B. 1985, in Solar Radiophysics: Studies of Emission from the Sun at Metre Wavelengths, ed. D. McLean & N. Labrum (Cambridge, Great Britain: Cambridge University Press), 333–359
Nindos, A., Aurass, H., Klein, K.-L., & Trottet, G. 2008, Sol. Phys., 253, 3
Pick, M., Démoulin, P., Krucker, S., Malandraki, O., & Maia, D. 2005, ApJ, 625, 1019
Plainaki, C., Belov, A., Eroshenko, E., Mavromichalaki, H., & Yanke, V. 2007, J. Geophys. Res., 112, 4102
Pohjolainen, S., van Driel-Gesztelyi, L., Culhane, J. L., Manoharan, P. K., & Elliott, H. A. 2007, Sol. Phys., 244, 167
Pomoell, J., Vainio, R., & Kissmann, R. 2008, Sol. Phys., 253, 249
Rieger, E., Treumann, R. A., & Karlický, M. 1999, Sol. Phys., 187, 59
Ruffolo, D. J., Saiz, A., Bieber, J. W., et al. 2010, AGU Fall Meeting Abstracts, A1814+
Ryan, J. M. 2000, Space Sci. Rev., 93, 581
Sáiz, A., Ruffolo, D., Bieber, J. W., Evenson, P., & Pyle, R. 2008, ApJ, 672, 650
Simnett, G. M. 2006, A&A, 445, 715

Simnett, G. M. 2007, A&A, 472, 309
Trottet, G., Vilmer, N., Barat, C., et al. 1998, A&A, 334, 1099
Vashenyuk, E. V., Balabin, Y. V., Perez-Peraza, J., Gallegos-Cruz, A., & Miroshnichenko, L. I. 2006, *Adv. Space Res.*, 38, 411
Vilmer, N., MacKinnon, A. L., Trottet, G., & Barat, C. 2003, A&A, 412, 865
Vršnak, B., Klein, K.-L., Warmuth, A., Otruba, W., & Skender, M. 2003, Sol. Phys., 214, 325